

Measurements of the Drift Velocity in Drift Velocity Chambers (VDC)

von

Jennifer Arps

Bachelorarbeit in Physik

vorgelegt der

Fakultät für Mathematik, Informatik und Naturwissenschaften der RWTH  
Aachen

im August 2010

angefertigt im

III. Physikalischen Institut A

bei

Prof. Dr. Thomas Hebbeker

Ich versichere, dass ich die Arbeit selbstständig verfasst und keine anderen als die angegebenen Quellen und Hilfsmittel benutzt sowie Zitate kenntlich gemacht habe.

Aachen, den 2. August 2010

# Contents

<b>1</b>	<b>Introduction</b>	<b>1</b>
1.1	The Large Hadron Collider (LHC) . . . . .	1
1.2	The Compact Muon Solenoid (CMS) Detector . . . . .	2
1.3	The Purpose of the Drift Velocity Chambers . . . . .	5
<b>2</b>	<b>Basics of Gas Detectors</b>	<b>8</b>
2.1	Energy Loss of Electrons . . . . .	8
2.2	Drift and Diffusion of Electrons in Gases . . . . .	9
2.3	Gas Avalanche . . . . .	10
<b>3</b>	<b>The Principle of Operating and Setup of the Drift Velocity Chambers</b>	<b>12</b>
3.1	The Principle of Operation of the VDCs . . . . .	12
3.2	Components and Electronics for the Determination of the Drift Velocity . . . . .	15
<b>4</b>	<b>Measurements of the Drift Velocity via Time to Digital Converter (TDC)</b>	<b>18</b>
4.1	Experimental Procedure to Determinate the Operation Point . . . . .	19
4.2	Analysis of the Measurements . . . . .	21
4.2.1	Analysis of the Rate at the Anode . . . . .	21
4.2.2	Analysis of the Number of Events that Are Used for the Determination of the Drift Time Difference . . . . .	21
4.2.3	Analysis of the Anode Current as a Function of the Anode Voltage . . . . .	25
4.2.4	Analysis of the Anode Noise Rate . . . . .	27
4.2.5	The Achieved Precision of the Drift Velocity in a 300 s Testing Time . . . . .	28
4.2.6	Analysis of After Pulses and Their Influence on the Drift Velocity Measurement	30
4.3	Error Calculation . . . . .	32
4.3.1	Statistical Error of Number of Events and of Rate . . . . .	32
4.3.2	Error of the Measured Drift Velocity . . . . .	32
<b>5</b>	<b>Conclusion and Outlook</b>	<b>34</b>

<b>Bibliography</b>	<b>35</b>
<b>A Statistic File</b>	<b>37</b>

# 1 Introduction

By resolving small structures the wavelength must have the same order of magnitude as the structure itself. Today's research focuses on the analysis of substructure of the size about 1/1000 the diameter of the proton that is 1 fm or  $10^{-15}$  m. Due to the Heisenberg uncertainty principle a very large momentum for forcing the particles to approach each other very closely is needed.

$$\Delta x \cdot \Delta p \geq \frac{\hbar}{2}. \quad (1.0.1)$$

In this formula  $\hbar$  is Planck's constant, which is  $6.6 \cdot 10^{-16}$  eVs,  $\Delta p$  is the uncertainty of the momentum and  $\Delta x$  is the space component. This is the foundation of accelerator physics.

The particles are accelerated by an electric field. After accelerating charged particles like electrons or protons they are brought to collision from an antiparallel beam or with a static target. If the particles collide with high energy, secondary particles are produced in the scattering process. This way it is possible to study the substructure of those accelerated particles. For such experimental studies precise particle detectors are needed. One of such detectors is the Compact Muon Solenoid Detector.

## 1.1 The Large Hadron Collider (LHC)

The Large Hadron Collider (LHC) is the most powerful and presently world's largest particle accelerator. It is situated in Geneva, Switzerland. The LHC is implemented in the tunnel of the former Large Electron Positron Collider (LEP) with a circumference of approximately 27 km. The LHC was built at the European Organisation for Nuclear Research (CERN) with the intention to test various predictions of high-energy physics and to search for the Higgs boson and other new particles.

The LHC is a synchrotron and therefore collides antiparallel proton beams at a center of mass energy of 7 TeV with a duration of two years. Afterwards the center of mass energy will increase to 14 TeV. The peak luminosity  $L$  will be about  $10^{34} \text{ cm}^{-2} \cdot \text{s}^{-1}$ . The beam is bent by 1232 superconducting dipole magnets, which are cooled down to 1.9 K and can create magnetic fields up to 8 T. Various particle detectors are placed at four intersection points of the particles' beams and points of collision, i.e. interaction points

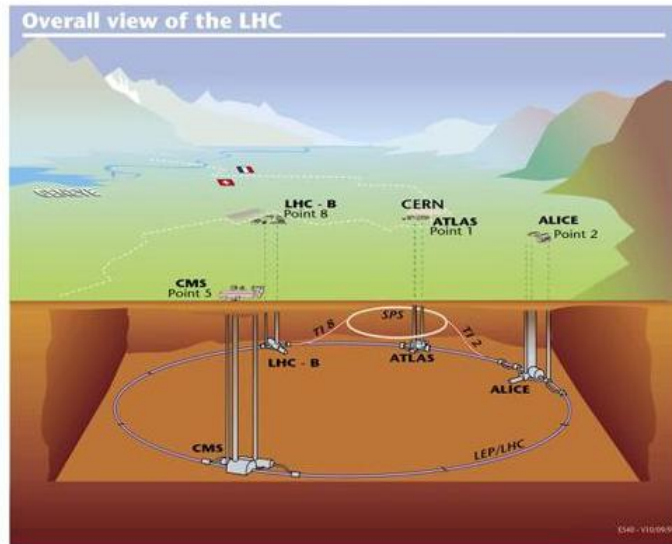


Figure 1.1: A view of the LHC with its four experiments [1]

[2]. Those four detectors and the whole LHC can be seen in Figure 1.1.

The four large experiments are ALICE (A Large Ion Collider Experiment), ATLAS (A Toroidal LHC ApparatuS), CMS (Compact Muon Solenoid) and LHCb (Large Hadron Collider beauty experiment). ALICE is a detector specialized in analysing lead-ion collisions instead of protons. LHCb experiment has the aim to measure the parameters of CP violation in the interactions of b-mesons (particles containing a bottom quark). CMS and ATLAS are multi-purpose particle physics detectors. Those two experiments will be able to mutually validate the results of each other [2].

## 1.2 The Compact Muon Solenoid (CMS) Detector

The Compact Muon Solenoid Detector (CMS) is subdivided into the so called barrel region and the end caps. The barrel region consists of the solenoid magnet, the tracker system and the calorimeters. Five large iron wheels hold the subdetectors and the muon system. In the iron wheels there are three cylindrical iron layers, that guide the magnetic field interspaced with chambers of the muon detector. The subdetectors and the solenoid magnet are constructed in concentric layers. Figure 1.2 gives an overview of the detector. The detector is centered around the interaction point, where the proton-proton collisions occur.

The magnet creates a magnetic field of about 4T inside the coil volume and the magnetic field is parallel to the LHC beam axis. Charged particles are deviated on a circle and it is possible to measure the momentum and the sign of the charge. The next subsections are about the five layers in which the

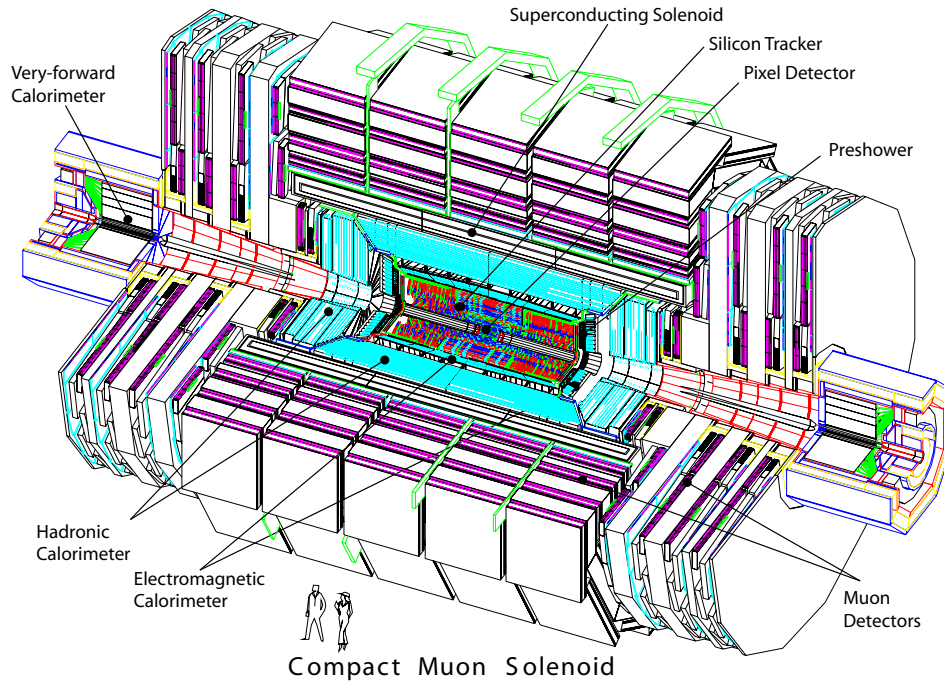


Figure 1.2: The setup of the CMS Detector. The interaction point is in the center of the detector. [3]

subdetectors and magnet are implemented.

The first layer consists of two subdetectors called silicon pixel tracker and silicon strip tracker. Close around the interaction point, there is the silicon pixel tracker, which can resolve a very high density of charged particles and determine precisely the vertex position for particles decaying close to the interaction point. The spatial resolution is about 0.01 mm. Around this silicon pixel tracker there is the silicon strip detector. It has a spatial resolution of better than 0.1 mm [4].

The second layer consists of the Electromagnetic Calorimeter (ECAL). This calorimeter can measure the energies of electrons, positron and photons with high accuracy. The ECAL, which is constructed from crystals of lead tungstate, in chemical notation  $\text{PbWO}_4$ , can also measure the energy deposited by charged hadrons. Just a fraction of the energy of the charged hadrons is deposited in the ECAL. In order to absorb the hadrons leaking out of ECAL, a further layer of calorimeter, called the Hadronic Calorimeter is needed.

The third layer consists of the Hadronic Calorimeter (HCAL). The HCAL is used to determine the energy of the hadrons, charged or neutral particles that are produced in each event. Besides, the HCAL has to be as close as possible to the interaction point, because it is supposed to measure hadrons also, which do not have high energy or a long lifetime. The calorimeter consists of dense material like brass or steel. This

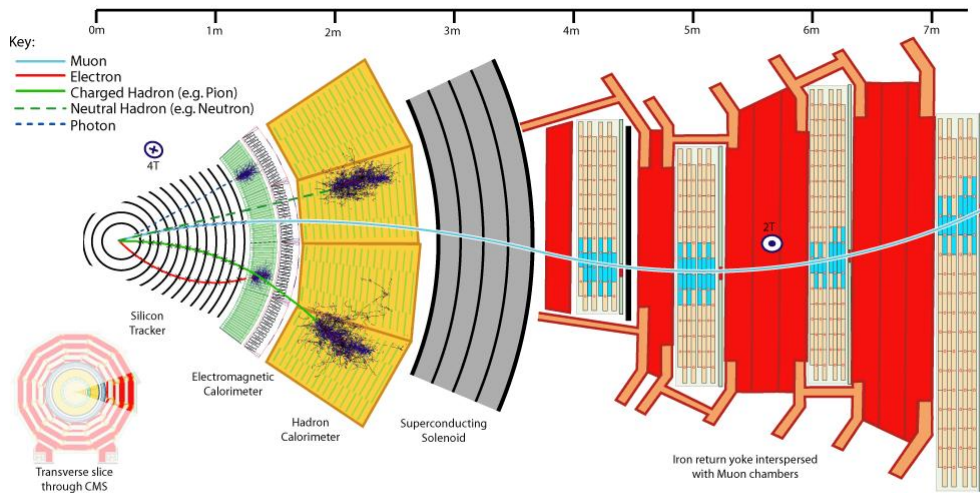


Figure 1.3: The profile of a slice of one wheel of the CMS Detector [5]. The five layers are schematic illustrated (f.l.t.r.): silicon pixel and silicon strip tracker, ECAL, HCAL, superconducting solenoid, muon subdetector system with the magnet yoke.

material works as absorber material and creates particle showers. Those showers are detected in plastic scintillators.

The fourth layer consists of the large solenoid magnet with a diameter of about 6 m. The magnetic field is generated by a 12.5 m long superconducting coil. The coil creates a magnetic field up to 4 T. This allows a high resolution measurement of the transverse momentum of charged particles [4].

The fifth layer consists of the muon subdetector system. Only muons and neutrinos can reach the muon chambers. Neutrinos hardly interact with matter. Therefore, the drift chambers of the muon system will locate the muon's path. The muon system is constituted of drift chambers ( $DT^1$ ,  $CSC^2$ ) and resistive plate chambers (RPC), interspaced with the iron yoke. Because of the iron wheels, there is only a small magnetic field in the muon chambers. The muons' curvature of path, which is a measure of its momentum, happens in the magnetized iron itself. From the interaction point of the beams, the particles have to cross very dense material. That is why only muons and neutrinos can reach the last layer and long tracks are available for momentum measurements.

For muon measurements various kinds of gas detectors are used. The principle of gas detectors is that charged particles ionize the gas in the detectors. The arising electrons and ions are detected by an anode

<sup>1</sup>Drift Tube

<sup>2</sup>Cathode Strip Chamber

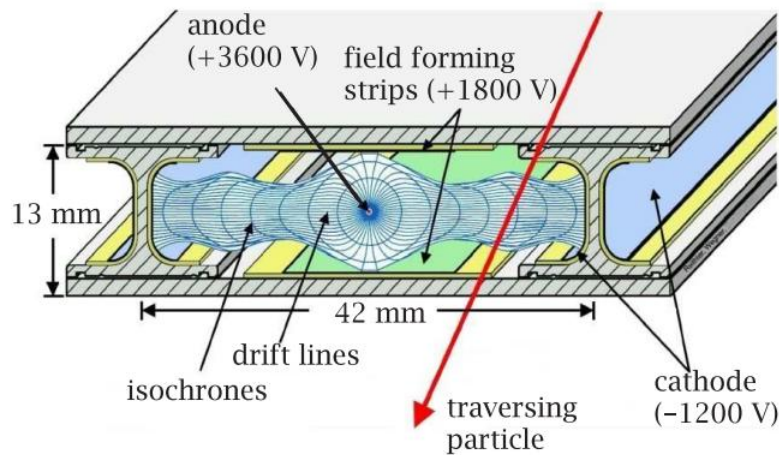


Figure 1.4: Drift Tube profile [6] with drift lines and isochrones for all paths of electrons, which end at the anode. The field strengths (200 - 250 V/mm) cause an almost constant drift velocity of  $55 \mu\text{m/ns}$ .

and cathode. More about the physical background of gas detectors can be read in the second chapter. At the barrel region DTs are placed. They are able to determine the position and the momentum of high energy muons. RPCs are mainly for triggering purposes but also for redundancy. They are positioned at the end caps and also at the barrel. In the end caps there are the CSCs. Also inside the end caps the magnetic field is very inhomogeneous and the density of particles is much higher there. This is why CSCs are used. Under this stringent conditions the CSCs are also able to deliver adequately precise position and time information. The muon chambers are implemented so that they overlap. For this reason there are no gaps and all muons can be captured.

### 1.3 The Purpose of the Drift Velocity Chambers

The basic unit of the muon system is the DT. This tube can be seen in Figure 1.4. In this figure two electrodes are at the edges that are the cathodes. The wire at the center of the tube is the anode and has a diameter of 0.05 mm. An electric field is generated with a drift field of  $100 \text{ V/mm}$  to  $250 \text{ V/mm}$  [4].

When a charged particle drifts towards the anode it causes an avalanche by gas amplification in a very high electric field close to the anode and generates a measurable electrical signal. In a DT the generated electrons drift towards the anode with an average drift velocity of  $v_d = 55 \mu\text{m/ns}$ . The distance of the track to the anode wire can be determined by measuring the time difference to an external trigger for example the RPCs. The combination of many drift tubes makes it possible to reconstruct the whole track of the

muons or generally charged particles.

In every barrel muon chamber a gas mixture of argon 85% and carbon dioxide 15% is used. The volume of the gas chambers is approximately  $1 \text{ m}^3$ . Making sure, that there is always sufficient clean gas inside the chamber, a gas flux of  $50 \text{ l/h}$  is used.

In the DTs the drift velocity is not always constant. This happens because the drift velocity depends on the type of gas, the gas' pressure and the electric field in the chamber. The gas can be polluted with air, water steam, halogens and silicates. There are a few methods to reduce these impurities. These can be sieves or an Oxisorb<sup>TM3</sup>, which can filter the oxygen and other gases but not nitrogen. The main problem is, that nitrogen is very similar in its chemical characteristics and size to oxygen but cannot be filtered chemically with comparable precision. Nitrogen, also in small concentration, influences the drift velocity massively. In Figure 1.5 the nitrogen influence on the drift velocity is shown. There can be seen that an impurity of 0.2 % of nitrogen causes a change of about 4 % in the drift velocity.

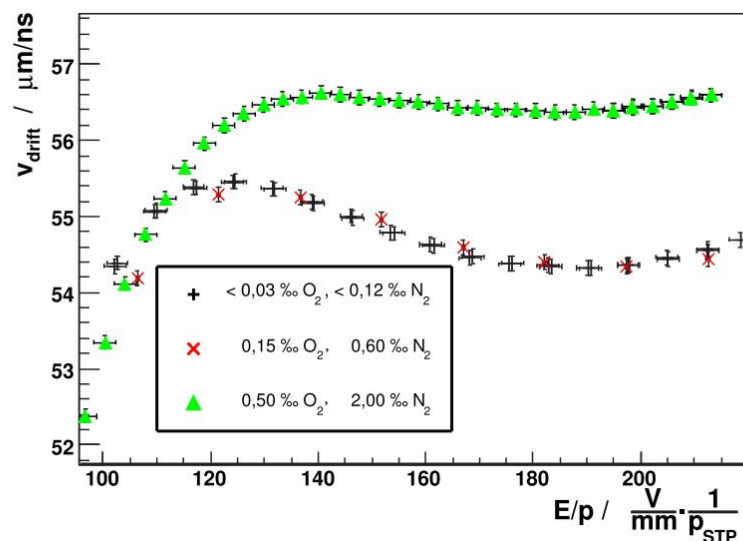


Figure 1.5: Measurements of the drift velocity in Ar/CO<sub>2</sub> with a small admixtures of 0.15 ‰ O<sub>2</sub>, 0.6 ‰ N<sub>2</sub> and 0.5 ‰ O<sub>2</sub>, 2 ‰ N<sub>2</sub> in comparison with clean gas (i.e. O<sub>2</sub> < 0.03 ‰, N<sub>2</sub> < 0.12 ‰) at constant pressure. A significant difference can be seen between the clean gas and the two mixtures especially due to nitrogen [7].

In order to ensure a continuous and precise monitoring of the drift velocity in the actual gas mixture of the DTs, a system of many sensors and Drift Velocity Chambers (VDCs) is designed.

Even if the correct gas mixture will be exactly known, the VDCs can measure the drift velocity with a higher precision than the DTs. In one wheel there are 50 muon chambers and there are five wheels in

<sup>3</sup>Messer Griesheim GmbH

total. With only one VDC ten days are needed for measuring the gas of all muon chamber in every wheel. This is why there will be six VDCs in the CMS Detector. One is for each wheel and the sixth is a spare.

## 2 Basics of Gas Detectors

Ionizing particles can be detected by gas detectors. When charged particles cross matter, they interact with it. There are several possibilities how charged particles can interact. Charged particles with kinetic energies below 10 MeV mainly interact with matter by ionization. The collision ionization of matter leads to free electrons from the shells of the atoms and positively charged ions. In an electric field the electrons drift to the anode and the ions to the cathode. With the help of gas amplification the incoming electrons can generate a measurable signal.

For heavy particles, e.g. muons, the energy-loss per distance  $\frac{dE}{dx}$  is described by the Bethe-Bloch-Formula [8]:

$$\left(\frac{dE}{dx}\right)_{ion.} = -F \cdot \frac{Z}{A} \cdot \rho \cdot \frac{1}{\beta^2} \cdot (\ln(\beta^2 \gamma^2) + C). \quad (2.0.1)$$

$$F = \frac{4\pi N \alpha^2 \hbar^2}{m_e} = 30 \text{ keV} \cdot \text{m}^2 / \text{kg}$$

$A$  = atomic mass of matter

$\beta = v/c$  here:  $v$  = velocity of the particle

$N$  = Avogadro constant

$I_{eff}$  = effective ionization energy in eV

$$C = \ln\left(\frac{2m_e c^2}{I_{eff}}\right)$$

$Z$  = atomic number of matter

$\rho$  = density of the matter

$\alpha$  = electromagnetic coupling constant

$m_e$  = mass of electron in eV/c<sup>2</sup>

$$\gamma = \frac{1}{\sqrt{1-\beta^2}}$$

### 2.1 Energy Loss of Electrons

Electrons are light particles. Their mass is for example 1/2000 of the proton's mass. Hence, electrons do not pass matter in a straight way but do multiple scattering like Möller-Scattering and Mott-Scattering or are slowed down in the electric field of nuclei (bremsstrahlung). Möller-Scattering is elastic scattering off shell electrons and Mott-Scattering is elastic scattering off nuclei. Therefore, the Bethe-Bloch-Formula

has to be modified for electrons. For relativistic electrons the following formula is a good approximation [9]:

$$\left(\frac{dE}{dx}\right)_{ion.} = -F \cdot \frac{Z}{A} \cdot \rho \cdot \frac{1}{\beta^2} \cdot \left(\frac{1}{2} \ln(\beta^2 \gamma^2) + D\right). \quad (2.1.2)$$

The constant  $D$  is approximately 7. Electrons with an energy of a few MeV are relativistic.

The critical energy  $E_c$  is the energy, at which the energy loss by ionization and bremsstrahlung are equal.

The Bethe-Bloch-Formula describes energy losses of relativistic electrons only until the critical energy.

For gas the formula is [8]:

$$E_c = \frac{710 \text{ MeV}}{Z + 0.92}. \quad (2.1.3)$$

By using argon, with  $Z = 18$ , the critical energy  $E_c$  is 37.5 MeV. In the VDCs the maximal energy of the Sr-90  $\beta$ -decay electrons is 2.28 MeV<sup>1</sup>, which is below the critical energy  $E_c$ . The energy loss of a Sr-90  $\beta$ -decay electron is dominated by ionization.

## 2.2 Drift and Diffusion of Electrons in Gases

By crossing a gas, electrons lose energy by collisions very quickly. Without the influence of an electric field, the electrons adopt the energy  $\varepsilon$  of the Maxwell-Boltzmann-Distribution [10]:

$$F(\varepsilon)d\varepsilon = C \cdot \sqrt{\varepsilon} \cdot e^{-\frac{\varepsilon}{k_B T}} d\varepsilon. \quad (2.2.4)$$

The constant  $k_B$  is the Boltzmann constant and  $T$  the temperature. The average energy  $\langle \varepsilon \rangle$  of this distribution is

$$\langle \varepsilon \rangle = \int_0^\infty \varepsilon F(\varepsilon) d\varepsilon = \frac{3}{2} \cdot k_B \cdot T \approx 0.03 \text{ eV} \quad (2.2.5)$$

<sup>1</sup>More about the Sr-90 decay energies is in section 4.1

at room temperature. The average velocity is  $\bar{v} = \sqrt{2 \cdot \varepsilon / m_e}$ .

In presence of an electric field, the electrons are accelerated in the direction of the field, gaining an additional velocity  $u = eE\tau/m_e$  between two collisions.  $\tau$  is the mean time between two collisions with atoms. For stronger fields the energy distribution is dominated by the energy gain between two collisions. Macroscopically, the effect of this additional velocity appears as the drift velocity  $v_d$ . The drift velocity is given by [11]:

$$v_d = \frac{2 eE}{3 m_e} \left\langle \frac{\lambda}{\bar{v}} \right\rangle + \frac{1 eE}{3 m_e} \left\langle \frac{d\lambda}{d\bar{v}} \right\rangle. \quad (2.2.6)$$

The mean free path  $\lambda$  is a function of the number of density  $N$  of the gas molecules and the scattering cross section  $\sigma(\varepsilon)$ :

$$\lambda = \frac{1}{N\sigma(\varepsilon)} \quad (2.2.7)$$

By using  $\lambda$  and  $\bar{v}$  the drift velocity  $v_d$  becomes:

$$v_d = \frac{1 eE}{3 m_e N} \left( \left\langle \sqrt{\frac{2m_e}{\varepsilon}} \frac{1}{\sigma(\varepsilon)} \right\rangle + \left\langle \sqrt{\frac{2m_e}{\varepsilon}} \varepsilon \frac{d}{d\varepsilon} \frac{1}{\sigma(\varepsilon)} \right\rangle \right). \quad (2.2.8)$$

For equation 2.2.8, the averaging is done over the energy distribution of the electrons. For small drift fields, the part in brackets becomes constant and by using the Ideal Gas Law  $pV = Nk_bT$  whereas  $p$  is the pressure, the drift velocity  $v_d$  is

$$v_d \propto \frac{E}{N} \propto \frac{ET}{p}. \quad (2.2.9)$$

## 2.3 Gas Avalanche

By crossing a gas, minimum ionizing particles create about ten electron-ion pairs per millimetre. These are not sufficient for sensing an electric signal. Here the gas avalanche in the large electric field near the anode wire provides the necessary amplification. At very high electric fields the drifting electrons may be accelerated so much between two collisions so that they have enough energy to create electron-ion

pairs. Those free electrons can ionize further molecules again. A cascade is created. If the avalanche factor  $G = N_{in}/N_{out}$  is up to  $10^6$ , a single electron can produce a signal up to a few mV on a wire read out by a coupling capacitor of 470 pF.

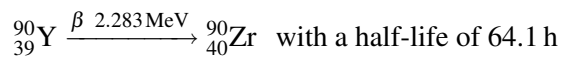
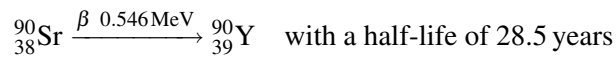
The electric field of a wire is proportional to  $1/r$  and  $r$  is the distance to the wire axis. Therefore, there is a very high electric field close to the wire. In a gas mixture of Ar/CO<sub>2</sub> (85:15), an anode voltage of 1850 V and the given geometry of the chamber the avalanche region (here 450 V/mm) begins in a distance of 1 mm from the wire.

## 3 The Principle of Operating and Setup of the Drift Velocity Chambers

The VDCs are constructed to monitor the CMS drift tube chambers. That is why the VDC-system must be able to validate the correctness of its own data. Every component of the VDCs must be controlled strictly. The VDCs have to measure the drift velocity of electrons in gas continuously. This VDC-system is not the first drift velocity monitoring system. A small special drift chamber for controlling the drift velocity, called “gas test chamber” was used to monitor a Time Expansion Chamber [12]. Improvements were needed, because at the CMS experiment much higher electric fields are used in the DTs.

### 3.1 The Principle of Operation of the VDCs

The outer size of the VDC is 200 mm x 120 mm x 100 mm. The inner volume is about one litre. Outside the chamber two Sr-90 sources are placed at a fixed distance of 48 mm as shown in Figure 3.1. The activity of each source is 10 MBq. The  $\beta$ -beams are generated by decays of Sr-90 [13].



The  $\beta$ -spectrum falls with the energy, and the mean  $\beta$ -energy amounts to about one third of the maximum energy. Most of the electrons from the first decay do not have enough energy to reach the scintillating fibre in the Trigger Unit, at the opposite side of the VDC (Figure 3.1), or to create enough light inside it. The electric field is shaped by field shaping electrodes. The electrodes are positioned in such way that there is a very homogeneous electric field in the middle of the chamber, the so called sensitive region. In this region the electric field  $E$  is about 200 V/mm with a homogeneity of  $\delta E/E \approx 0.1\%$  [14].

In front of the  $\beta$ -sources there is a collimator for each beam. It has a diameter of 1 mm and a length of 17 mm. At the opposite side of the VDC there are two rectangular collimators with width and length

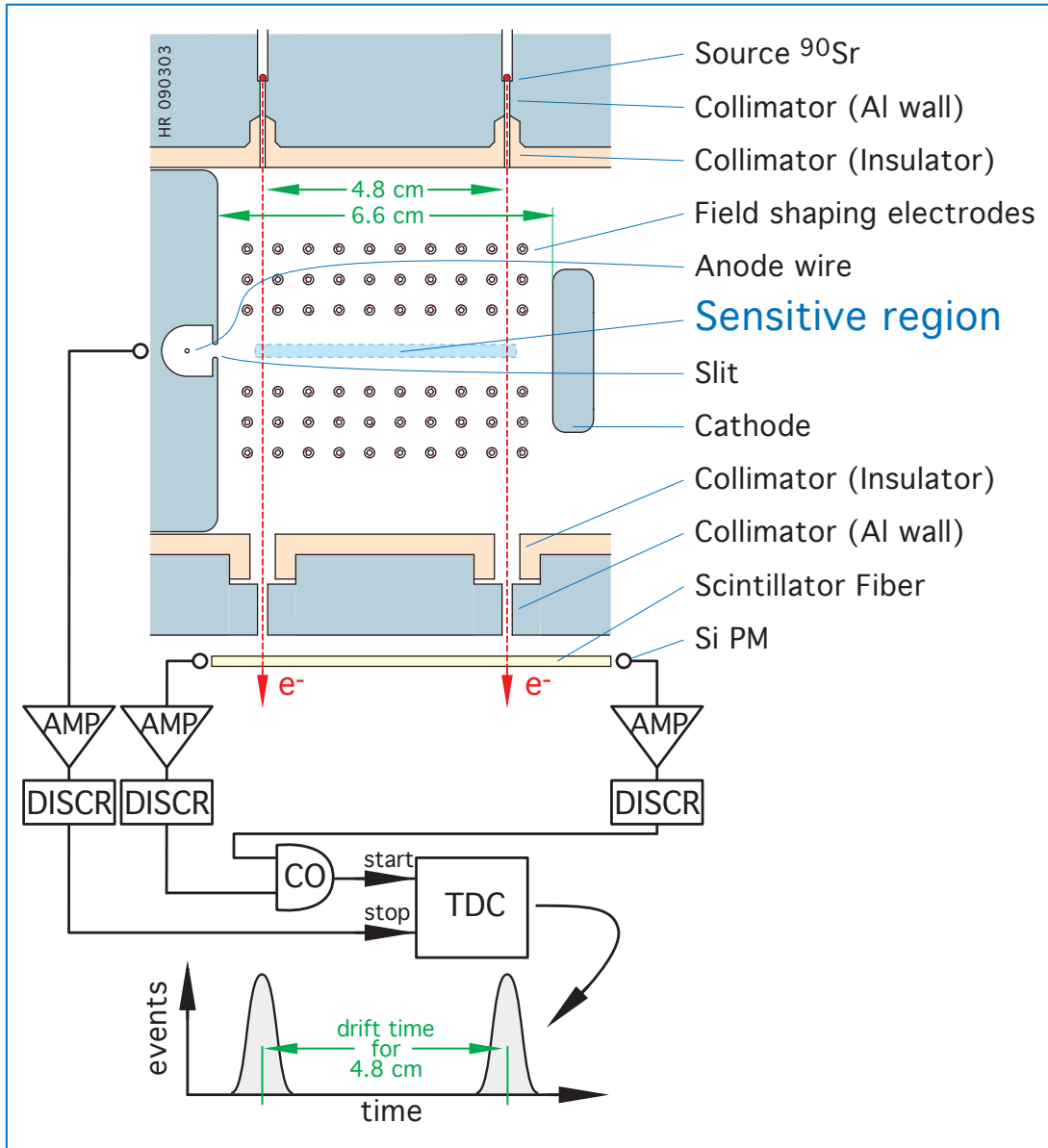


Figure 3.1: The principle of operation of a VDC [6]

of 2 mm x 10 mm. The collimator points to the scintillating fibre<sup>1</sup> (Figure 3.5) connected to two silicon photomultipliers (short: SiPMs<sup>2</sup>).

Due to the geometry of the collimators in front of the sources the  $\beta$ -beams are projected to a circle. Thus, only a fraction of the  $\beta$ -decay electrons of the 10 MBq sources cross the chamber. With no absorption in the source encasement and gas,  $\beta$ -decay electrons with a rate of 2162 Hz for each source are expected to cross the chamber. For both sources the rate is 4325 Hz. The  $\beta$ -decay electrons ionize the gas in the chamber. The electrons generated by ionization travel to the anode. Hence, the expected rate at the anode is approximately 4325 Hz. In contrast the  $\beta$ -decay electrons travel to the collimators at the opposite side of the VDC. The collimators are at a distance of 75 mm from the sources, so that the  $\beta$ -beam of the source has a diameter of 5.4 mm. Due to the geometry of the collimators and the fact that only  $\beta$ -decay electrons with energies greater than 1.2 MeV can reach the scintillating fibre [14], 8 % of the  $\beta$ -decay electron rate (4325 Hz) hits the scintillating fibre, i.e. 338 Hz. Neglecting multiple scattering and the detection efficiencies, this estimate gives only a rough benchmark.

The anode voltage is set between 1850 V and 2000 V. The anode room is separated from the drift room by a 2.5 mm wide slit. Hence, only the electrons from this 2.5 mm wide sensitive region can reach the anode while every other electron is stopped at the field shaping electrodes or the chamber walls. Thus, only the electrons which drift through the most homogeneous part of the electric field are taken into account for the determination of the drift velocity. At the anode the arriving electrons provide a measurable signal by charge amplification due to the high electric field near the anode. This signal is amplified, digitized and sent to a TDC<sup>3</sup> that measures the time between the start signal from the coincidence of the SiPMs signals and the arrival of the drift electrons at the anode.

Filling a histogram with many of those time measurements, a drift time spectrum is created. There are two peaks as indicated in Figure 3.2. Those peaks represent the two drift times  $t_1$  and  $t_2$  for the path from the two ionizing  $\beta$ -beams to the anode wire.  $t_1$  represents the drift time of the electrons, that are ionized by the  $\beta$ -decay electrons of the left source in Figure 3.1 (the distance to the anode is shorter for the left source than for the right source).  $t_2$  represents the drift time of the right source. Due to the homogeneous electric field in the region between both beams, the drift velocity is constant and can be calculated to:

$$v_d = \frac{\Delta x}{t_2 - t_1} = \frac{\Delta x}{\Delta t}. \quad (3.1.1)$$

---

<sup>1</sup>Type of fibre: BCF-12 MC

<sup>2</sup>SiPM-type: Hamamatsu MPPC 1 mm<sup>2</sup> S10362-11-100C

<sup>3</sup>Time to Digital Converter, here a digital multihit VME module of type V767B from CAEN.

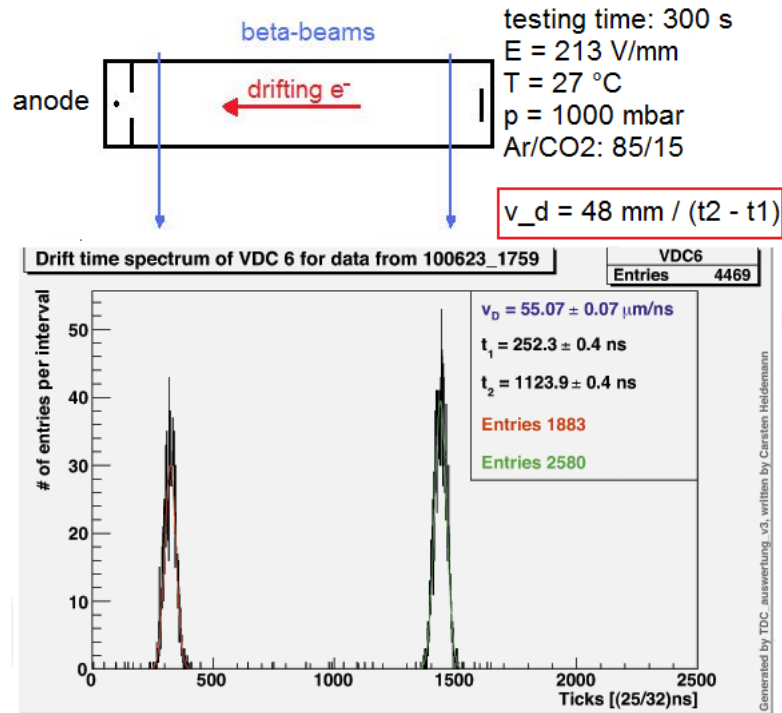


Figure 3.2: Drift time spectrum as an example for calculating the drift velocity. For this spectrum only the first anode signal is taken (cf. subsection 4.2.6).

$\Delta x$  is the distance of the two radioactive sources. Near the anode there are unavoidable inhomogeneities of the electric field that affect both time measurements in the same way and are “cancelled out” by using  $\Delta t$ .

### 3.2 Components and Electronics for the Determination of the Drift Velocity

In the rack at the left-hand side of Figure 3.3 there is a VME-crate with the main part of the trigger logic and a NIM-crate with part of the trigger logic. Also there are the six VDCs, which are located at the lower part of the rack at the right-hand side of the figure. The PC is for the acquisition and analysis of the data and for performing measurements. The adjustable high voltages are delivered by the high voltage-crate<sup>4</sup>. The working voltage is  $-14 \text{ kV}$ <sup>5</sup>. With this voltage an electric field of approximately  $212 \text{ V/mm}$ <sup>6</sup> is generated, which is nearly the largest field strength in the drift tube of the muon chambers.

For measuring the drift velocity a start signal and a stop signal is needed. The  $\beta$ -decay electrons, reach

<sup>4</sup>High voltage-crate type: CAEN SY1527, with supply modules A1526N (cathode HV), A1821P (anode HV) and A1510 (for SiPMs)

<sup>5</sup>High voltage power supply type: CAEN A1526N

<sup>6</sup>More information can be found in a diploma thesis [14]

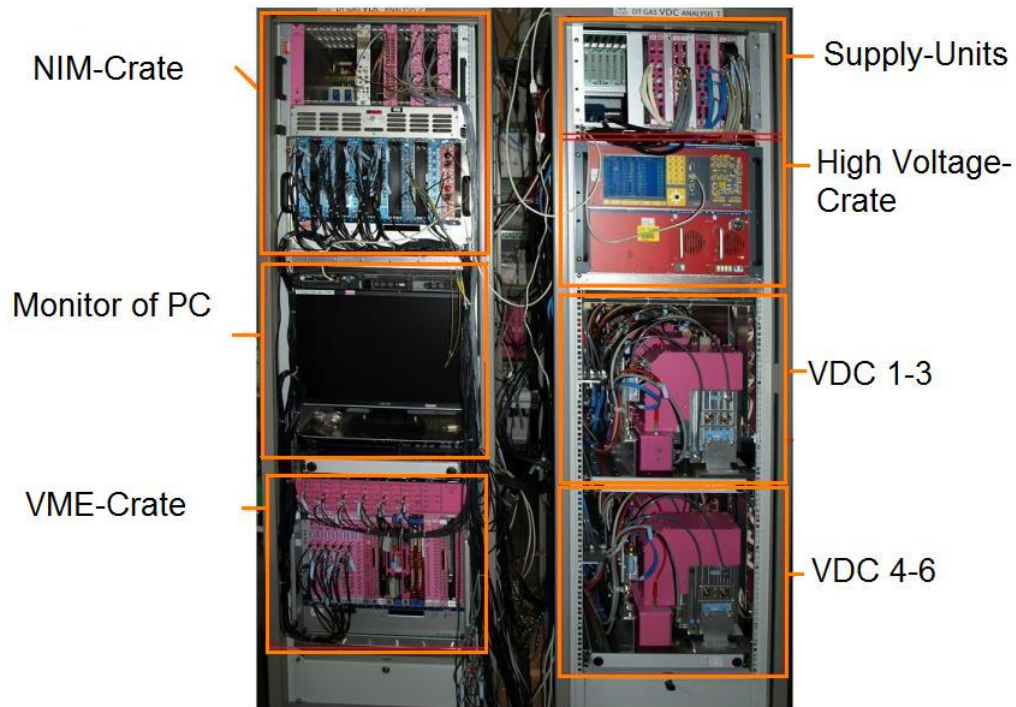


Figure 3.3: The VDC system and its components in Aachen [15]

the collimator at the opposite side of the chamber, strike the 1 mm x 1 mm rectangular scintillating fibre. The scintillating fibre is connected to the SiPMs in u-shape. A schematic illustration of the fibre can be seen in Figure 3.5. One electron creates photons in the scintillating fibre which diffuse in all directions in the fibre and are detected at both SiPMs. Fibre, SiPMs and preamplifier are in the Trigger Unit. At first the signals are amplified by a preamplifier. Then a discriminator converts the signals, which pulse amplitudes exceed a predefined threshold, to NIM-pulses.

The trigger logic (Figure 3.4) creates an additional fourth signal to the three signals (SiPM1, SiPM2, anode). This fourth signal is the coincidence of the two SiPMs. The coincidence is the start signal of the drift time measurement. The stop signal comes from the anode. A preamplifier in a box is mounted on the anode side of the chamber. A discriminator module, located in the NIM crate, generates a NIM-pulse (width 25 ns), if the absolute pulse amplitude exceeds a predefined threshold. The NIM-pulses are converted to ECL-pulses by a digital NIM-to-ECL converter. Then the TDC registers all signals arriving within a predefined window of 1.25  $\mu$ s before and 1.25  $\mu$ s after the trigger signal.

The trigger signal from all six chambers are connected by OR and are delivered to the trigger channel of the TDC. If an event is registered at the trigger, the relative times of the events  $t_1$  and  $t_2$  will be saved as an event in the output storage of the TDC. Only if the four signals (SiPM1, SiPM2, anode and trigger) from a VDC are registered, they will be recognized as a complete event.

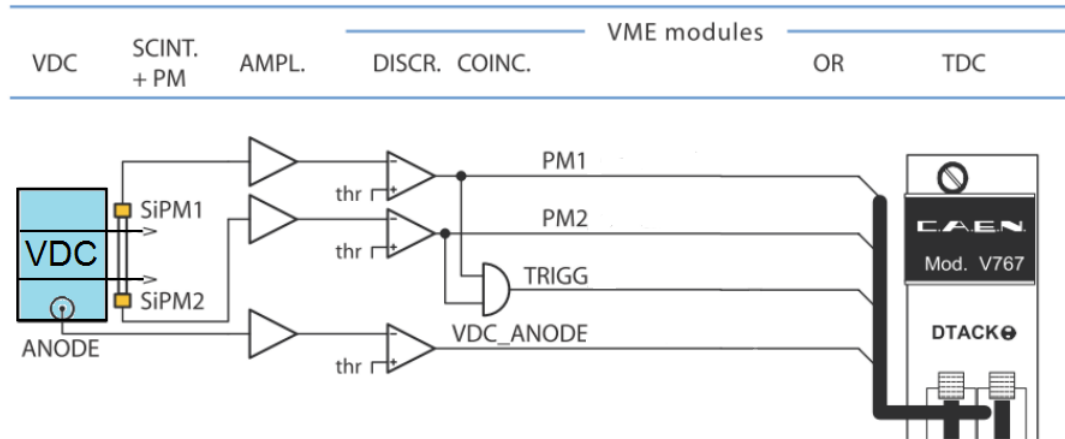


Figure 3.4: Trigger and digitizing logic. [6]

Additionally to the TDC there are two external counter modules<sup>7</sup>. In contrast to the TDC which only counts the anode signals in a predefined time window, the counter counts every anode signal. The counter also counts the SiPM1, SiPM2 and the trigger signals.

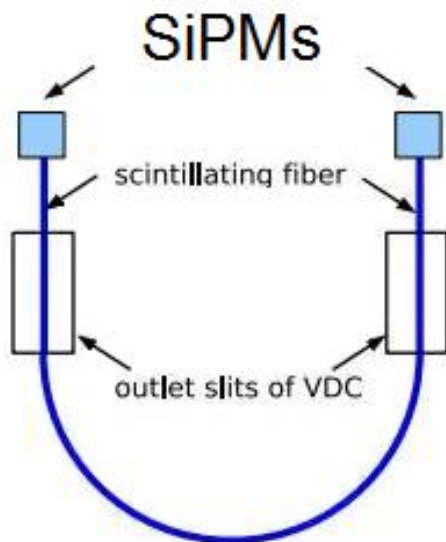


Figure 3.5 [7]: On both endings of the scintillating fibre there are the SiPMs that have a 1 mm x 1 mm sensitive area. The preamplifier is inside the Trigger Unit, while the discriminator and the coincidence are in the VME modules. The TDC detects the times from the coincidence, the SiPM1, SiPM2 and the anode. The reason for using one fibre is that the noise from the two SiPMs is eliminated by requiring a coincidence of their signals. More about the start signal generation can be found in a bachelor thesis [16].

<sup>7</sup>CAEN V560

## 4 Measurements of the Drift Velocity via Time to Digital Converter (TDC)

This thesis is about the measurement of the drift velocity. They are used to determine the optimal anode voltage for each chamber. Furthermore, it is interesting to know, which thresholds have to be set up at the anode's discriminator and at the SiPMs' discriminator. Another important point of the analysis is the number and shape of after pulses. They will influence the mean value of the gauss fit in the drift time spectrum if the fit region includes after pulses. When the optimal thresholds and anode voltages are known, it is possible to determine the drift velocity very efficiently, i.e. precisely and quickly.

An optimal voltage of the anode is needed, because the number of produced pulses is an exponential function of the anode voltage. A too low voltage would cause a low efficiency of detecting the arriving drift electrons. A too high voltage would cause too much noise pulses. Additionally photoelectrons will be created in the material around the anode due to UV photons. Another important effect is that space charge can build a shield charge around the anode wire which limits the avalanche development in the gas. The operation point includes the optimal anode and SiPMs voltages and the thresholds of the discriminators. The optimal SiPM voltages are determined in [16]. The operation point can be recognized by considering the following aspects:

- high event rates that are independent of small variations of the voltages
- the corresponding anode current should be in the order of 20 nA observed at lower voltage (cf. subsection 4.2.3)
- small amounts of noise and after pulses

Overall this thesis is analysing the VDCs<sup>1</sup> 2, 3, 4 and 6.

---

<sup>1</sup>s is for indicating the serial number. VDCs 2, 3, 4, 6 were installed at the position p 2, 3, 4, 6, respectively, in the rack, together with Trigger Unit number 2, 7, 4, 6

## 4.1 Experimental Procedure to Determinate the Operation Point

To determine the operation point of high voltage and of discriminator threshold setting for the anode and the SiPMs, following measurement programs are carried out. The measurement program type of run “ANODE” is the following: The anode voltage is increased in equal intervals of 20 V from 1740 V to 1980 V, while the voltages at the SiPMs kept constant. The SiPM voltages, set for these runs, are shown in Table 4.1. These are the operation voltages of the SiPMs given by the manufacturer<sup>2</sup>.

VDCs	VDCp	trigger unit	SiPM1	SiPM2
2	2	2	70.0 V	69.9 V
3	3	7	69.9 V	69.6 V
4	4	4	70.0 V	70.0 V
6	6	6	69.4 V	69.4 V

Table 4.1: SiPM voltages that are used in all measurements. VDCs is the serial number, while VDCp is the position of the VDC in the rack.

At each anode voltage the incoming events at the SiPMs, the trigger and at the anode are measured for 300 s with the counter and the TDC. The 300 s measurement time is for some VDCs too short with respect to the aim of the VDCs that the measured drift velocity should have a precision better than 1 %. This precision should be reached in about 10 min which is of the same order of magnitude as the time a VDC is planned to be connected to the outlet of a muon chamber. Nevertheless, the main characteristics of the measured time distribution, that means how many complete events and the width of the peak, can already be seen in 300 s.

At every anode measurement point the drift velocity is calculated and a drift time spectrum is plotted. For the present studies the set of thresholds listed in Table 4.2 for type of run “ANODE” is used.

anode threshold/ SiPMs thresholds		
0.05/ 0.1	0.05/ 0.2	0.05/ 0.3
0.1/ 0.1	0.1/ 0.2	0.1/ 0.3
0.2/ 0.1	0.2/ 0.2	0.2/ 0.3
0.3/ 0.1	0.3/ 0.2	0.3/ 0.3

Table 4.2: Measurement program with absolute thresholds in Volt. Left is assigned the anode threshold and right the SiPMs thresholds.

Additionally, noise measurements are made, i.e. type of run “ANODE” was used with the same set up but without radioactive sources.

The following measurements are performed at an electric field of 212 V/mm. In this region the drift ve-

---

<sup>2</sup>Hamamatsu

locity is expected to vary with the electric field at a rate of  $0.036 \mu\text{m}\cdot\text{ns}^{-1}/\text{V}\cdot\text{mm}^{-1}$ , see Figure 4.1. The inhomogeneity of the electric field is 1.5‰ along the central path of the electrons in the sensitive region and below 3‰ at a symmetrical distance of 4 mm around the central path axis [14]. Actually the electrons that make their way to the anode do not reach the area 4 mm away from the central path. In the worst case, i.e. the inhomogeneities are not symmetrical around the path axis, the error of  $v_d$  at an electric field of  $200 \text{ V}/\text{mm}$  is around 0.3‰. This is the reason why the large DT chambers are operated in this area of the electric field, in which the drift velocity varies only moderately with the electric field, and the reason that the measurements of the drift velocity are made at an electric field of  $212 \text{ V}/\text{mm}$  in this thesis.

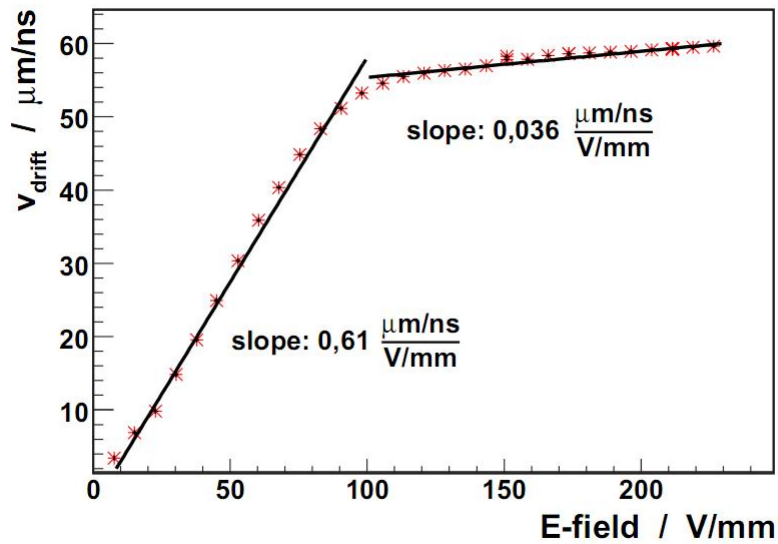


Figure 4.1: The measured drift velocity in dependence on the electric field. [7]

The laboratory conditions for all measurements are a gas pressure  $p$  of 1000 mbar and a temperature  $T$ , in the gas room, of approximately  $27^\circ\text{C}$  in the VDCs.

For the analysis of the TDC data a special statistic file is created for each drift time spectrum. In this statistic file the TDC data is analysed regarding the number of triggered events, the number of missing anode signals for all triggered events, the number of events in the drift time spectrum and many more. An example of such a statistic file is shown in the appendix.

## 4.2 Analysis of the Measurements

### 4.2.1 Analysis of the Rate at the Anode

By analysing the anode rate at every measured voltage by a type of run “ANODE” measurement, it is possible to determine the coarse operation point of the anode. The counting time is 500 s at every voltage. The operation voltage can be defined as the point where a plateau starts, see Figure 4.2. At low anode voltages there are only a few anode pulses which can pass the discriminator threshold and hence the rate is not high enough. At higher voltages the gas avalanches become larger and the rate increases. At the plateau every electron is detected and so the rate does not increase anymore. The noise rate also increases at higher anode voltages. To detect every electron but have a minimum of noise pulses, the operation point should be at the plateau.

Measured is the trigger, which is represented by the black curve. This has to be constant because the voltages of the SiPMs are kept constant at type of run “ANODE”. The blue curve is the rate of accidental coincidence<sup>3</sup>, which is lower than the black curve at the set up SiPM voltages (Table 4.1). The red curve is the anode rate. The plateau starts at 1840 V and ends at approximately 1920 V. This coarse area of the operation point is for each chamber the same. In this figure the anode rate is 2000-3000 Hz at the plateau, which agrees with the estimate in section 3.1. In the next section the number of events for calculating the mean of the two drift times  $t_1$  and  $t_2$  are analysed in the possible area of the operation point that means between 1840-1920 V.

The statistical errors thus lead to error bars smaller than the dots in Figure 4.2. The statistical error of each rate is  $\sqrt{N}/500$  s.  $N$  is the number of signals measured in 500 s.

### 4.2.2 Analysis of the Number of Events that Are Used for the Determination of the Drift Time Difference

For the determination of the drift times  $t_1$  and  $t_2$  the results from the gauss fits to the two peaks are used. The number of complete events (2 SiPMs, anode, trigger) used for the gauss fits are the red and green number in Figure 3.2. High red and green numbers are an indication that many complete and correct events are registered at the TDC. In this subsection it is analysed at which thresholds and anode voltages the number of events used for the gauss fits is the highest. Additionally, it is analysed at which thresholds and anode voltages the number of unused events is high, i.e. incomplete events and events that are not in the gauss fits. Incomplete events are events with less than four entries. Mainly incomplete events are triggered events with missing stop signal (anode signal) in the time window  $1.25 \mu$  s before and after

---

<sup>3</sup>More about the accidental coincidence is in a bachelor thesis [16]

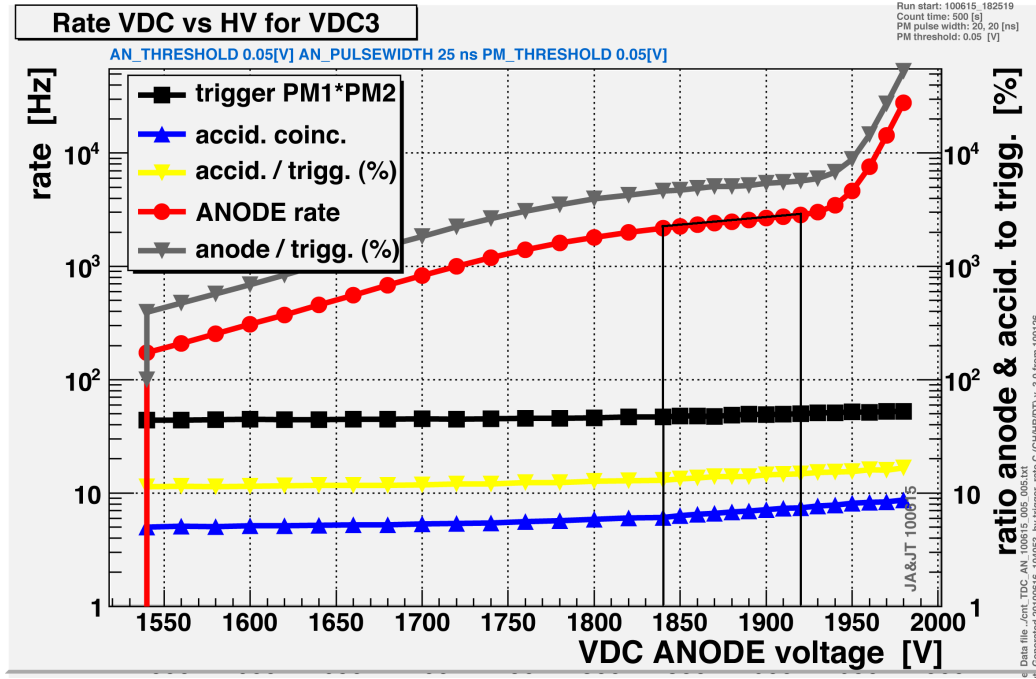


Figure 4.2: Type of run “ANODE” for VDCs 3, it is measured 500 s at each point. Anode threshold 0.05 V, SiPMs thresholds 0.05 V. Pulse width 20 ns. Conclude that the operation voltage is between 1840-1920 V. The anode rate is significantly higher than the trigger rate, because only a small fraction of the  $\beta$ -particles pass the collimator and hit the narrow scintillating fibre of the trigger unit.

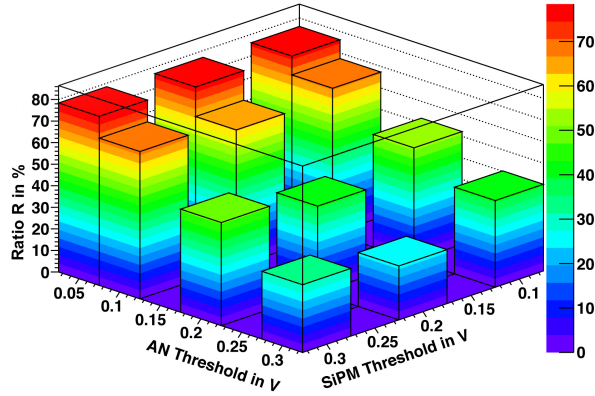
triggering. Unused events have to be avoided, because these indicate an incorrect set up of the operation point.

For this analysis the relevant variables are:

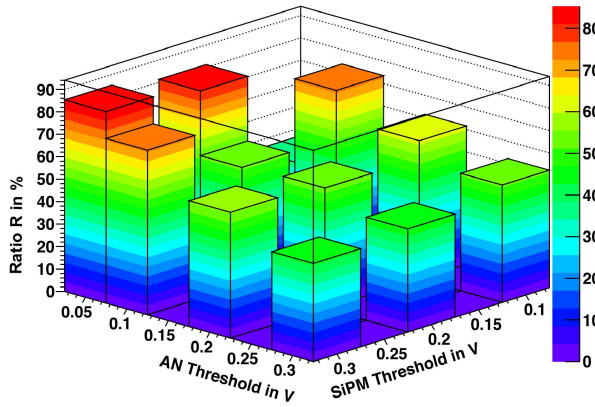
1. All events used for the gauss fits (red + green number in drift time spectrum) :=  $U$
2. All triggered events :=  $T$
3. The ratio of  $U/T$  :=  $R$
4. All unused events  $T - U$  :=  $UU$

In Figure 4.3 the ratio  $R$  is shown as a function of the applied discriminator thresholds for the SiPMs and the anode exemplary for the VDC 6. Each plot is for one anode voltage which is at the plateau in Figure 4.2 for a testing time of 300 s.

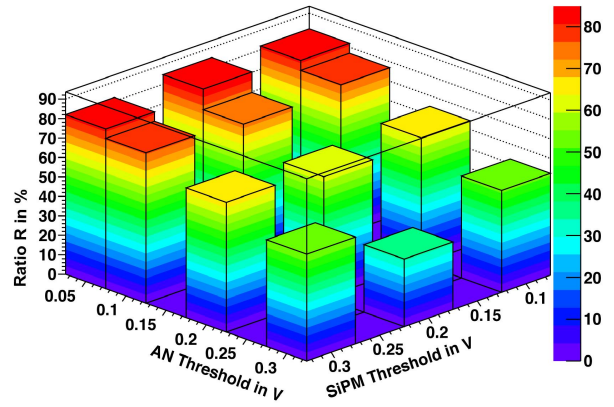
The ratio  $R$  is always the highest for an anode threshold of 0.05 V at any anode voltage. With regard of the SiPM thresholds, the ratio  $R$  is always the highest for SiPM thresholds of 0.03 V or 0.02 V. At  $U_A = 1920$  V, at an anode threshold of 0.05 V and at a SiPM threshold of 0.3 V, the highest value of 89.3 % is observed for this ratio  $R$ .



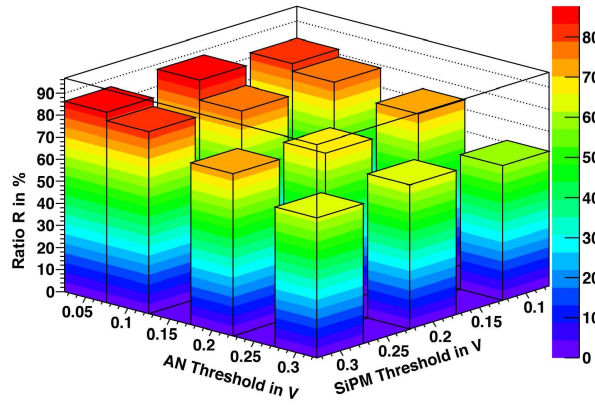
a)  $U_A = 1840$  V



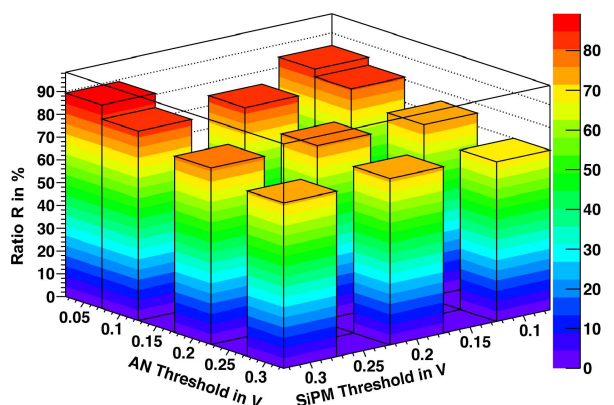
b)  $U_A = 1860$  V



c)  $U_A = 1880$  V



d)  $U_A = 1900$  V



e)  $U_A = 1920$  V

Figure 4.3 a)-e): Ratio  $R$  of the number of used VDC signals to the number of all registered triggers as a function of discriminators thresholds, for several values of the anode voltage exemplary for the VDC 6. The ratio  $R$  is the highest (89.3 %) at  $U_A = 1920$  V, at an anode threshold of 0.05 V and at a SiPM threshold of 0.3 V.

In Figure 4.3 e) one entry is missing, because there were no entries in the TDC data but the anode, trigger, and SiPM rates were counted correctly by the external counter. This happens sometimes. The reason for this is unclear, but the sources of error could be e.g. a malfunction of the TDC or a loose connection at the TDC module. Further measurements have shown that after touching the TDC module some data may be missing (or suddenly reappear).

In Figure 4.3.b) there is one entry, which percentage is not as estimated. It is only 36.5 % at an anode threshold of 0.05 V and a SiPMs threshold of 0.1 V. This percentage is normalised to 300 s, because the measurement, in the TDC data registered, was only 200 s. It would be expected that this entry would be more than 70 % as the trend shows. This short measurement time is an indication that this measurement failed. The read out of the signals must be blocked in the TDC. One possible explanation cannot be given at the moment.

Now, it has to be analysed, whether  $U$ , all events used for the gauss fits, is also the highest at the highest ratios  $R$ .  $U$  and  $UU$  for the runs of Figure 4.3 are listed in Table 4.3. Since the runs had the same duration, these number of events can be directly compared.

AN THR: SiPM THR:	0.3 V 0.1 V	0.2 V 0.1 V	0.1 V 0.1 V	0.05 V 0.1 V
$U_A = 1840$ V: $U/ UU$	2124/ 3159	2914/ 2664	3972/ 1920	1541/ 484
$U_A = 1860$ V: $U/ UU$	2829/ 2584	3592/ 2238	1961/ 702	65/ 113
$U_A = 1880$ V: $U/ UU$	2838/ 2592	1374/ 758	4162/ 1252	2573/ 566
$U_A = 1900$ V: $U/ UU$	3327/ 2123	2490/ 859	1761/ 476	2994/ 651
$U_A = 1920$ V: $U/ UU$	3369/ 1444	1523/ 486	2447/ 575	4082/ 747
	0.3 V 0.2 V	0.2 V 0.2 V	0.1 V 0.2 V	0.05 V 0.2 V
$U_A = 1840$ V: $U/ UU$	659/ 1979	1178/ 1745	2006/ 1170	2476/ 744
$U_A = 1860$ V: $U/ UU$	1215/ 1434	1522/ 1314	2155/ 1948	2638/ 607
$U_A = 1880$ V: $U/ UU$	874/ 1597	1820/ 1112	2227/ 771	2717/ 482
$U_A = 1900$ V: $U/ UU$	1670/ 886	2044/ 891	2437/ 653	2885/ 405
$U_A = 1920$ V: $U/ UU$	1896/ 702	2302/ 691	2554/ 520	-/ -
	0.3 V 0.3 V	0.2 V 0.3 V	0.1 V 0.3 V	0.05 V 0.3 V
$U_A = 1840$ V: $U/ UU$	580/ 1269	853/ 934	1096/ 509	1132/ 323
$U_A = 1860$ V: $U/ UU$	806/ 1031	977/ 769	1170/ 426	1339/ 232
$U_A = 1880$ V: $U/ UU$	1022/ 844	1127/ 566	1170/ 346	1271/ 279
$U_A = 1900$ V: $U/ UU$	596/ 344	1179/ 426	1340/ 287	1226/ 195
$U_A = 1920$ V: $U/ UU$	1312/ 501	1351/ 394	1302/ 265	1349/ 162

Table 4.3: Number of used  $U$  and unused  $UU$  events from VDC 6, as recorded by the TDC, for the conditions of Figure 4.3.

By considering this table the highest number of used events  $U$  for the VDC 6 is at  $U_A = 1920$  V, at an anode threshold of 0.05 V and a SiPMs threshold of 0.1 V. The trend is that the highest number of used events  $U$  is always at the lowest thresholds, as it is expected. To what extent the noise increases is anal-

used in subsection 4.2.4. The obtained results for all VDCs can be seen in Table 4.4. The statistical errors of the number of events are  $\sqrt{N}$ ,  $N$  is the number of events, and the error of the ratio  $R$  is calculated by error propagation.

	$U_A$ in V	AN_thr in V	PM_thr in V	$R$ in %	$U$	$UU$
VDC2	1920	0.05	0.2	$53.3 \pm 1.2$	$3320 \pm 58$	$2908 \pm 54$
VDC3	1900	0.05	0.1	$57.8 \pm 0.9$	$2245 \pm 47$	$1623 \pm 40$
VDC4	1920	0.05	0.2	$6.2 \pm 0.3$	$519 \pm 23$	$7877 \pm 89$
VDC6	1920	0.05	0.1	$84.5 \pm 1.4$	$4463 \pm 67$	$817 \pm 29$

Table 4.4: The operation point for all VDCs. VDC 4 has a low ratio  $R$  and many unused events  $UU$ .

Noticeable is the fact that VDC 4 has less events  $U$  than the other VDCs. Besides, VDC 4 has many unused events  $UU$ . This is very typical for VDC 4. Almost every incomplete event of VDC 4 is caused by a missing anode signal for a triggered event.

number of anode pulses in 1.25 $\mu$ s before and after one trigger (for 8384 triggered events)		
0	1	$\geq 2$
7865	519	approx. 2

Table 4.5: Number of anode pulses in a time window 1.25  $\mu$ s before and after a trigger at 8384 triggered events in 300 s testing time,  $U_A = 1920$  V, an anode threshold of 0.05 V and a SiPM threshold of 0.2 V for VDC 4. 94 % of the triggered events are without an anode signal (stop signal).

For 8384 triggered events in a 300 s measurement, 7865 anode pulses are missing. More about the fact that there is more than one anode signal in one time window of the trigger can be read in subsection 4.2.6. By comparing the anode rates with the other chambers it is noticeable, that VDC 4 has a smaller anode rate and a higher trigger rate than the other ones. As an exemplary visualisation: In a measurement with  $U_A = 1920$ , an anode threshold of 0.05 V and a SiPM threshold of 0.2 V (operation point of VDC 4) and by only regarding the rates from the counter, the anode rate is 31 times higher than the trigger rate at VDC 4. For VDC 6, in the same measurement, the anode rate is 219 times higher than the trigger rate. All in all it can be said, that the anode rate has to be greater than 31 times the trigger rate to collect enough statistics for an adequate drift time spectrum in little time (300 s).

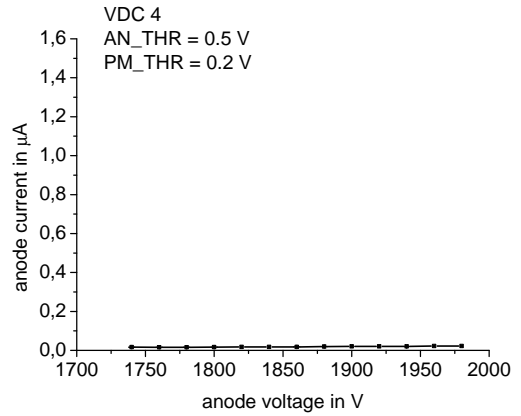
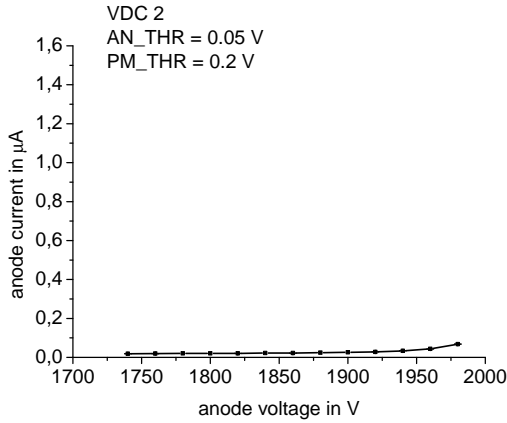
### 4.2.3 Analysis of the Anode Current as a Function of the Anode Voltage

The current of the anode  $I$ , increases with the applied voltage. At high voltages the anode current soars, which could cause damage, and has to be analysed especially in view of the operation voltages, see Table 4.4.

The following coarse numbers give an estimate of the order of magnitude for the anode current [6]:

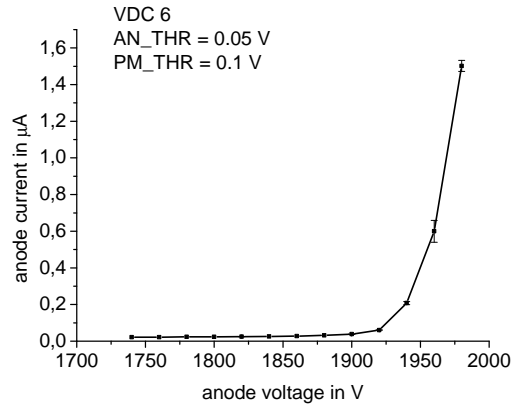
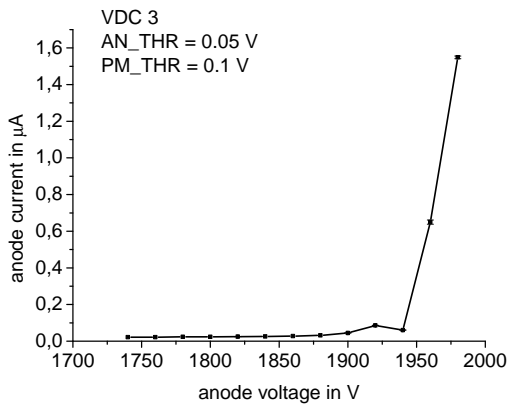
For 25 primary electrons from one ionizing particle, with a gas avalanche of a factor  $10^6$ , and for an anode rate of 5 kHz (including noise), the expected current  $I$  will be:

$$I = \frac{Q}{t} = \frac{e^- \cdot 25 \cdot 10^6}{2 \cdot 10^{-4} \text{ s}} \approx 20 \text{ nA.} \quad (4.2.1)$$



a) anode threshold of 0.05 V, SiPM threshold 0.2 V

b) anode threshold of 0.05 V, SiPM threshold 0.2 V



c) anode threshold 0.05 V, SiPM threshold 0.1 V

d) anode threshold 0.05 V, SiPM threshold 0.1 V

Figure 4.4 a)-d): Anode current as a function of the anode voltages for each chamber. It is visible that a dangerous increase of the current, i.e. a current much higher than 20 nA, is not given for the operation point for each chamber. VDC 4 operates probable at higher anode voltages, because the anode current is still low, while the anode current increases at  $U_A = 1940$  V at the other VDCs.

In Figure 4.4 the anode current  $I$  of each chamber is plotted as a function of the anode voltage. The error of the anode current is the standard deviation of multiple measurements of the anode current in 300 s at each measured voltage.

At  $U_A = 1740$  V the anode voltage is very low, so that the corresponding anode current is not in a critical area (much higher than 20 nA) that means in an optimal operation area. A comparison of the current at the operation point with the anode current at 1740 V for each chamber is given in Table 4.6.

	$I(1740 \text{ V})$ in $\mu\text{A}$	$I(\text{operation point})$ in $\mu\text{A}$	$I(\text{operation point})/I(1740 \text{ V})$
VDC2	$0.018 \pm 0.001$	$0.028 \pm 0.001$	1.6
VDC3	$0.022 \pm 0.001$	$0.045 \pm 0.001$	2.1
VDC4	$0.016 \pm 0.001$	$0.020 \pm 0.001$	1.25
VDC6	$0.022 \pm 0.001$	$0.060 \pm 0.001$	2.7

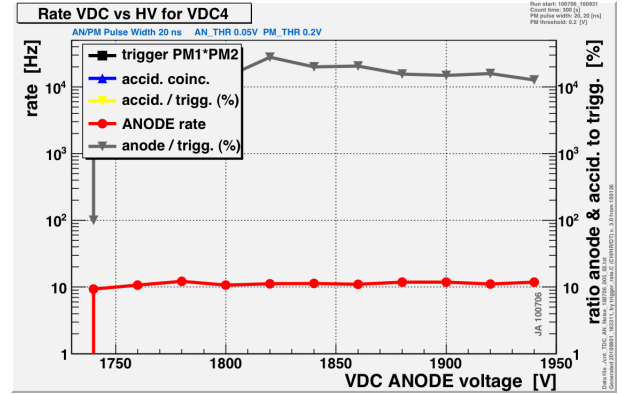
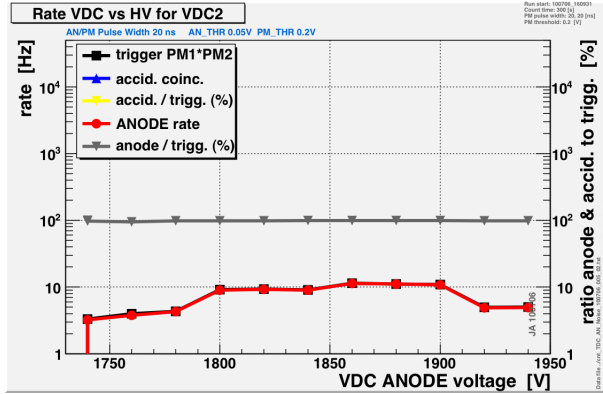
Table 4.6: Comparison of the anode current at low anode voltages ( $U_A = 1740$  V) with the anode current at the operation point. As it is visible in the third column the anode current at the operation point is maximum 2.7 times higher.

From these measurements it can be concluded, that at the selected operation point of Table 4.6 the anode currents are within a reasonable range and not too close to the steep slope of the anode current curve. The anode current curve of VDC 4 does not show the steep increase observed for the other VDCs. An explanation could be, that VDC 4 operates at higher anode voltages than the other VDCs. This could also explain the observed low statistics of VDC 4.

#### 4.2.4 Analysis of the Anode Noise Rate

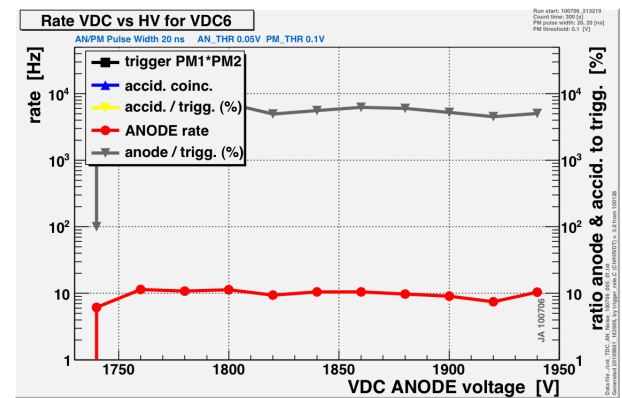
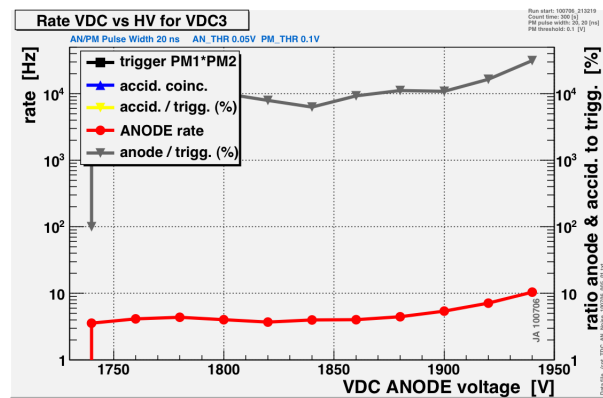
In the following measurements the anode noise rate, that means the anode rate without sources, is analysed. The noise measurements are made for 300 s at each measurement point. The rates of the anode curves, see Figure 4.5, show that the noise does not increase with the voltage, instead a constant anode rate is visible. A possible explanation is that the noise is very small and is overlayed by a constant cosmic radiation [6], but this is only an assumption and needs further analysis.

The anode/trigger-curve of VDC 3, 4, 6 shows that the expected trigger (coincidence) rate is 0.1 Hz and cannot be seen in the plot as it is invisible in the plots of VDC 3, 4 and 6. Noticeable is VDC 2. At VDC 2 the trigger rate is as high as the anode rate. The rates in Figure 4.5 are from the counter module and not from the TDC data. By analysing the TDC data of VDC 2 the noise of the trigger is of the same order of magnitude (that means of the correct order of magnitude) than the other VDCs. It can be concluded that the counter does electronic cross-talk between the anode and the trigger channel.



a) anode threshold of 0.05 V, SiPM threshold of 0.2 V

b) anode threshold of 0.05 V, SiPM threshold of 0.2 V



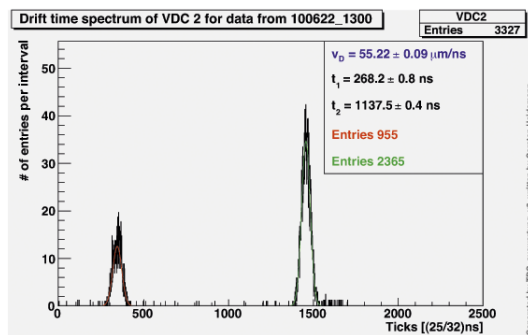
c) anode threshold of 0.05 V, SiPM threshold of 0.1 V

d) anode threshold of 0.05 V, SiPM threshold of 0.1 V

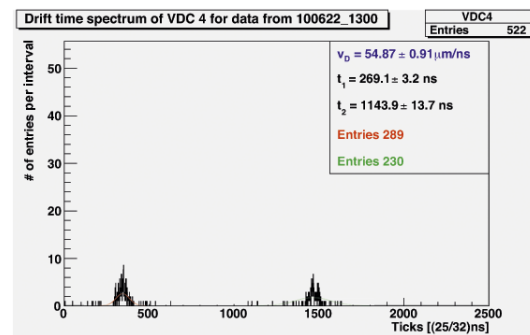
Figure 4.5 a)-d): Noise measurements of the anode without sources at the operation points. The constant anode rate is a hint for cosmic radiation, but this has to be further analysed. VDC 2: electronic cross-talk between trigger and anode rate in the counter module.

#### 4.2.5 The Achieved Precision of the Drift Velocity in a 300 s Testing Time

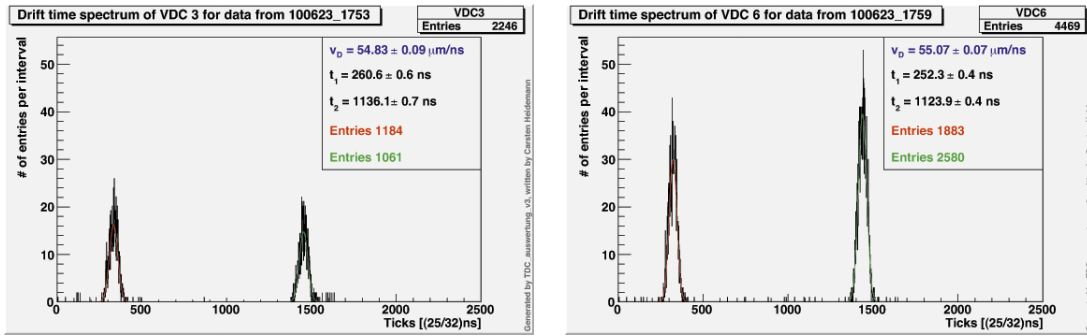
In Figure 4.6 the drift time spectra of each chamber can be seen at their operation points. The testing times are 300 s, the gas pressure  $p$  is 1000 mbar and the temperature  $T$  is about 27 °C in the gas room.



a)



b)



c)

d)

Figure 4.6 a)-d): The drift time spectra at the operation point for each chamber. SiPM/Anode Pulse width 20 ns, testing time 300 s,  $T$  approximately 27 °C and  $p$  is 1000 mbar. In these drift time spectra always the first anode pulse is taken (cf. subsection 4.2.6). a), b)  $U_A = 1920$  V, anode threshold of 0.05 V, SiPM threshold of 0.2 V. c)  $U_A = 1900$  V, anode threshold of 0.05 V, SiPM threshold of 0.1 V. d)  $U_A = 1920$  V, anode threshold of 0.05 V, SiPM threshold of 0.1 V The height of the first peak of VDC 2 is almost half of the second peak. VDC 4 has low statistics.

In the drift time spectra the peaks have a width. The different arrival times of the electrons created by ionization at the anode which leads to the width, are mainly because of the inhomogeneity of the drift field.

Only complete events are filled in the drift time spectra. For the drift time determination only the first anode signal of one event is taken (cf. subsection 4.2.6). The red and the green curves in Figure 4.6 are gauss fits at each peak. The mean value of the gauss fits are the drift times  $t_1$  and  $t_2$ . The limits of integration of the first peak are 0 to 500 ticks. The limits of integration of the second peaks are 1000 to 1700 ticks. One tick is approximately 0.78 ns. In Figure 4.6 it is not visible, but the limits of the x-axis are 0 and approximately 1700 ticks. 1700 ticks match with 1.33  $\mu$ s. This time window of 1.33  $\mu$ s represents the 1.25  $\mu$ s-time window, that is before and after a trigger, with a delay of 0.08  $\mu$ s. This delay can be explained by the additional delay due to the connection by OR of the trigger signals. The errors of the time measurements are taken from the gauss fit. The determination of the error of the drift velocity  $v_d$  is explained in section 4.3.

Noticeable is that the first peak of VDC 2 is lower than the second peak (Figure 4.6 a)). The first peak is approximately the half of the height of the second peak. This is the case in every measurement. A possible explanation cannot be given at the moment. Besides this, VDC 4 has very low statistics. Incomplete events are the reason for the low statistic. Mainly the anode signal is missing. As mentioned above, the reason seems to be that the operation point of VDC 4 is at a higher voltage than used here.

	$v_d$ in $\mu\text{m/ns}$	$\sigma_{v_d}$ in $\mu\text{m/ns}$	$\sigma_{v_d}/v_d$ in %
VDC2	55.22	0.09	0.16
VDC3	54.83	0.09	0.16
VDC4	54.87	0.91	1.66
VDC6	55.07	0.07	0.13

Table 4.7: Measured drift velocity and estimated error. Measurement at selected operation point for anode voltage and thresholds of anode and SiPMs. If the relative error is  $< 1\%$  in a measurement time of 300 s, the VDCs will have enough events, that means the operation point is optimal set up. The drift velocities are equal within  $3\sigma$ .

All in all the error of the drift velocity  $\sigma_{v_d}$  obtained for a run of 300 s is below 1 % for every chamber besides VDC 4.

To compare the drift velocity of each chamber the following formula gives the difference between two velocities, in units of the expected standard deviation:

$$N_\sigma = \frac{v_{d,x} - v_{d,y}}{\sqrt{\sigma_{v_d,x}^2 + \sigma_{v_d,y}^2}}. \quad (4.2.2)$$

The drift velocity measurements are under the same conditions, but by using equation 4.2.2, the drift velocities of VDC 2, 3 and VDC 3, 6 are equal within  $3\sigma$ . VDC 2, 6 are equal within  $2\sigma$  and every VDC is with VDC 4 within  $1\sigma$  due to the fact of the low statistics of VDC 4. All in all, first indications of a similar drift velocity is given by the VDCs. By repeating the drift velocity measurements under same conditions, possible systematic errors of the drift velocity can be determined.

#### 4.2.6 Analysis of After Pulses and Their Influence on the Drift Velocity Measurement

In addition to the uniformly distributed background in a drift time spectrum, after pulses are visible (Figure 4.7 b)). It is possible that more than one anode signal is registered in the time window  $1.25\mu\text{s}$  before and after a trigger. After pulses are caused by more than one anode signal. There are two kinds of after pulses. The first kind of after pulse is of electronic origin. An electronic after pulse may arise, if the circuit begins to oscillate. The second kind of after pulse is caused by UV photons that produce photoelectrons in the material of the anode room at high electric fields. By deciding which anode signal is to be used for calculating the mean value of the drift times  $t_1$  and  $t_2$ , the result of the gauss fit might change and therefore the drift velocity, too. In the following analysis the drift velocity obtained by taking the first anode signal is compared to the result obtained by taking the last anode signal for every trigger is compared. In both cases accidental noise hits would give a systematic bias to either earlier or later drift

times. For background hits from after pulses, only the method of taking the first hit from every event would be free of bias. As an estimate: If a complete event has more than one anode signal in the preset time window, on average the number of anode signals will be two.

In Table 4.8 the drift velocity  $v_d$  obtained by taking the first anode signal with the drift velocity obtained by taking the last anode signal is compared. Differences can be seen. The differences in the drift velocity between two VDCs is larger than the effect of the drift velocity by after pulses.

	$v_d$ in $\mu\text{m/ns}$ from the first anode signal	$v_d$ in $\mu\text{m/ns}$ from the last anode signal
VDC2	$55.22 \pm 0.09$	$55.18 \pm 0.09$
VDC3	$54.83 \pm 0.09$	$54.84 \pm 0.09$
VDC4	$54.87 \pm 0.91$	$54.84 \pm 0.87$
VDC6	$55.07 \pm 0.07$	$55.09 \pm 0.07$

Table 4.8: Comparison of the drift velocity by taking the first or the last anode pulse of one trigger at the operation point for each chamber

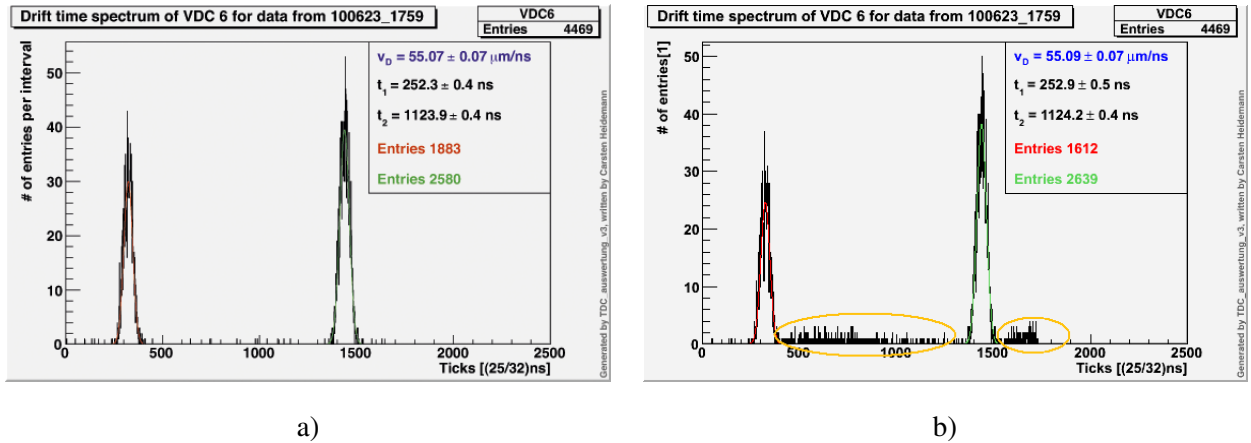


Figure 4.7: Selection of hits to be used for the calculation of the drift velocity.  $U_A = 1920$  V, anode threshold of 0.05 V, SiPM threshold of 0.1 V,  $T = 27$  °C,  $p = 1000$  mbar, testing time 300 s. a) Drift time spectrum of VDC 6 by taking the first signal of the anode. b) Drift time spectrum of VDC 6 by taking the last anode signal of every event. a) is the same as in Fig. 4.6 and has no after pulses and almost no background hits. b) the after pulses can be clearly seen (after pulses are marked orange).

The first peak of Figure 4.7.a) has 271 entries more than the first peak of Figure 4.7.b). 271 entries of 1883 entries are events with more than one anode signal. This estimate does not apply for the second peaks in Figure 4.7, because in Figure 4.7.b) the second peak could take entries from the 271 entries. It can be concluded that by taking only the first anode signal, the after pulse rate can be successfully eliminated.

## 4.3 Error Calculation

### 4.3.1 Statistical Error of Number of Events and of Rate

When counting a number  $N$  of events from a radioactive decay, the statistical uncertainty of this random process is given by  $\sigma = \sqrt{N}$ .  $N$  is the number of events. If a rate is measured and the error of the rate is needed, than the error is  $\sigma/t$ . The time  $t$  means the time in which  $N$  were measured. There is also a digitalization error of the time, but the error is in comparison to the order of magnitude of events too small to have a significant effect of the poisson error and can be neglected.

### 4.3.2 Error of the Measured Drift Velocity

The statistical error of the drift velocity is composed of the statistical error of the time and of the drift distance  $s$ .

The error of the CNC milling machine is estimated to 0.02 mm [6]. The distance  $s$  is the effective distance between the two beams of the radioactive sources at the sensitive region (Figure 3.1), calculated as the mean of the distance of the sources and the distance between the two scintillator segments in the trigger unit. Due to  $s_{rr}^4 = s_{ss}^5 = s_1 - s_2$  and  $s = (s_{rr} + s_{ss})/2$  and error propagation the absolute error of  $s$  is with  $\sigma_{s_{rr}} = \sigma_{s_{ss}} = 0.028$  mm:

$$\sigma_s = \sqrt{\frac{1}{2} \cdot (\sigma_{s_{rr}}^2 + \sigma_{s_{ss}}^2)} = 0.028 \text{ mm.} \quad (4.3.3)$$

The statistical error of the mean of time ( $\sigma_{t_1}, \sigma_{t_2}$ ) is taken from the gauss fit to each peak of the time distribution calculated by root<sup>6</sup>.

Calculating  $v_d$  as:

$$v_d = \frac{s}{t_2 - t_1} \quad (4.3.4)$$

The corresponding statistical error is:

$$\sigma_{v_d} = \sqrt{\left(\frac{s}{(t_2 - t_1)^2} \cdot \sigma_{t_1}\right)^2 + \left(\frac{s}{(t_2 - t_1)^2} \cdot \sigma_{t_2}\right)^2 + \left(\frac{1}{t_2 - t_1} \cdot \sigma_s\right)^2}. \quad (4.3.5)$$

---

<sup>4</sup>rr is for the distance between the two radioactive sources

<sup>5</sup>ss is for the distance between the two scintillator slits at the trigger unit

<sup>6</sup><http://root.cern.ch/drupal/>

The error of the distance  $\sigma_s$  is treated as a statistical error in equation 4.3.5, but for the single chamber it is a systematic error. The total error of the drift velocity  $\sigma_{v_d}$ , that is shown in every drift time spectrum, is calculated by addition of the relative error of the distance  $s$  approximately 0.059 % and the relative error of the time  $\Delta t = t_2 - t_1$ ,  $\sigma_{\Delta t} = \sqrt{\sigma_{t_1}^2 + \sigma_{t_2}^2} / \Delta t$ , because the systematic error of the distance  $s$  cannot be propagated in a gaussian way.

## 5 Conclusion and Outlook

All in all the operation points of VDCs 2, 3 and 6 are successfully determined and shown in Table 4.4. Aiming for precisions better than 1 % in a 10 min testing time is achieved for VDCs 2, 3 and 6. The precision of the measured drift velocity is estimated to be 0.2 % in a 5 min testing time for VDCs 2, 3 and 6 whereas the precision of VDC 4 is not better than 1 % in a 10 min testing time. A possible explanation is that VDC 4 needs higher voltages than the other VDCs.

The anode currents corresponding to the operating points have an acceptable value that means the anode current does not increase to damaging values. The anode noise-rate measurements show that the noise rate is constant. This could be an indication for cosmic radiation that overlays the actual noise rate.

The analysis of the after pulses shows that possible after pulses can be eliminated by taking only the first anode signals into account. It can be concluded that with the help of the operation points the efficiency of the VDCs is increased.

As an outlook, the following should be further analysed. VDC 4 has to count more events in general. That means the anode rate must be higher, because anode entries are always missing by TDC events for VDC 4. VDC 2 has to be investigated regarding that in the drift time spectra, always the first peak is much lower than the second peak. Afterwards with the help of simultaneous testing of six VDCs the systematic error can be determined for each chamber.

## Bibliography

- [1] <http://lhcatome.cern.ch/lhc/lhc.shtml>
- [2] <http://cdsmedia.cern.ch/img/CERN-Brochure-2008-001-Eng-2.pdf>
- [3] [http://cms.web.cern.ch/cms/Resources/Website/Media/Images/Detector/DetectorDrawings/fromGEANT/cms\\_complete\\_labelled.pdf](http://cms.web.cern.ch/cms/Resources/Website/Media/Images/Detector/DetectorDrawings/fromGEANT/cms_complete_labelled.pdf)
- [4] The CMS Collaboration, “The Muon Project-Technical Design Report”, CERN/L-HCC 97-32, December 1997. [http://cms.cern.ch/iCMS/jsp/page.jsp?mode=cms&action=url&urlkey=CMS\\_TDRS](http://cms.cern.ch/iCMS/jsp/page.jsp?mode=cms&action=url&urlkey=CMS_TDRS)
- [5] [http://cms.web.cern.ch/cms/Resources/Website/Media/Videos/Animations/files/CMS\\_Slice.gif](http://cms.web.cern.ch/cms/Resources/Website/Media/Videos/Animations/files/CMS_Slice.gif)
- [6] Hans Reithler, private communication, III. Physikalisches Institut A, RWTH Aachen, 2010.
- [7] Jens Frangenheim, “Measurements of the drift velocity using a small gas chamber for monitoring of the CMS muon system”, Diploma Thesis, III. Physikalisches Institut A, RWTH Aachen, 2007.
- [8] Particle Data Group, Review of particle physics, W-M Yao et al 2006 J. Phys. G: Nucl. Part Phys. 33 1
- [9] Kleinknecht, Teilchendetektoren, 4. Auflage, 2005, ISBN 978-3835100589
- [10] C. Grupen, “Particle Detektors”, Cambridge University Press, 2008.
- [11] R. C. Fernow, “Introduction to Experimental Particle Physics”, Cambridge University Press, 1986.
- [12] A. Böhm et al, “Experience with the L3 vertex drift chamber at LEP”, Nucl. Instrum. Methods Phys. Res. A, 2003.
- [13] <http://www.nndc.bnl.gov/> oder <http://www.stuarthunt.com/Downloads/RMSDS/Sr90.pdf>
- [14] Georg Altenhöfer, “Development of a Drift Chamber for Drift Velocity Monitoring in the CMS Barrel Muon System”, Diploma Thesis, III. Physikalisches Institut A, RWTH Aachen, 2006.
- [15] Carsten Heidemann, “Direkte Messung der Driftgeschwindigkeit im Gas der CMS-Myonkammern mit VDC-Kammern”, Diploma Thesis, III. Physikalisches Institut A RWTH Aachen, 2010.

- [16] Jenny Tempeler, “Measurements of the Trigger Rate in Drift Velocity Chambers”, Bachelor Thesis, III. Physikalisches Institut A RWTH Aachen, 2010.

## A Statistic File

The analysis program, that is written by Carsten Heidemann, creates a statistic file for every drift time spectrum. In these files the TDC data is analysed regarding the number of entries of SiPM1, SiPM2, trigger and anode signals that the TDC counts for every chamber. The measurement of the statistic file below is made at  $U_A = 1840$  V, an anode threshold of 0.05 V and a SiPM threshold of 0.3 V.

```

v_Drift VDCp1 : 0.00 +/- 0.00 um/ns
v_Drift VDCp2 : 55.13 +/- 0.18 um/ns
v_Drift VDCp3 : 54.95 +/- 0.22 um/ns
v_Drift VDCp4 : 55.77 +/- 15.49 um/ns
v_Drift VDCp5 : 0.00 +/- 0.00 um/ns
v_Drift VDCp6 : 55.02 +/- 0.13 um/ns

Weighted mean:
55.04 +/- 0.09 um/ns

Measurement started 2010-06-22 11:25:17
Measurement stopped 2010-06-22 11:30:25
Measurement runtime: 300 s

Event counts:

Global events for all chambers: 10888

Global events without trigger for all chambers: 0

Global events with multiple trigger entries for all chambers: 0

Global events with multiple trigger entries for VDC 1: 0
Global events with multiple trigger entries for VDC 2: 0
Global events with multiple trigger entries for VDC 3: 0
Global events with multiple trigger entries for VDC 4: 0
Global events with multiple trigger entries for VDC 5: 0
Global events with multiple trigger entries for VDC 6: 0

Global empty events: 24

Events identified to belong to VDC 1: 0
Events identified to belong to VDC 2: 2935
Events identified to belong to VDC 3: 1254
Events identified to belong to VDC 4: 5086
Events identified to belong to VDC 5: 0
Events identified to belong to VDC 6: 1613

Events with less 4 entries, not empty for VDC 1: 0
Events with less 4 entries, not empty for VDC 2: 1872
Events with less 4 entries, not empty for VDC 3: 644
Events with less 4 entries, not empty for VDC 4: 4959
Events with less 4 entries, not empty for VDC 5: 0
Events with less 4 entries, not empty for VDC 6: 237
Events with less 4 entries, not empty, all VDCs and not assigned: 7712

Events with missing trigger for VDC 1: 0
Events with missing trigger for VDC 2: 0
Events with missing trigger for VDC 3: 0
Events with missing trigger for VDC 4: 0
Events with missing trigger for VDC 5: 0
Events with missing trigger for VDC 6: 0

Events with missing PM1 for VDC 1: 0
Events with missing PM1 for VDC 2: 0
Events with missing PM1 for VDC 3: 0
Events with missing PM1 for VDC 4: 0
Events with missing PM1 for VDC 5: 0
Events with missing PM1 for VDC 6: 0

Events with missing PM2 for VDC 1: 0
Events with missing PM2 for VDC 2: 0
Events with missing PM2 for VDC 3: 0
Events with missing PM2 for VDC 4: 0
Events with missing PM2 for VDC 5: 0
Events with missing PM2 for VDC 6: 0

Events with missing AN for VDC 1: 0
Events with missing AN for VDC 2: 1872
Events with missing AN for VDC 3: 644
Events with missing AN for VDC 4: 4959
Events with missing AN for VDC 5: 0
Events with missing AN for VDC 6: 237

Events with at least one trigger and zero TDC, for VDC 1: 0
Events with at least one trigger and zero TDC, for VDC 2: 0
Events with at least one trigger and zero TDC, for VDC 3: 0
Events with at least one trigger and zero TDC, for VDC 4: 0
Events with at least one trigger and zero TDC, for VDC 5: 0
Events with at least one trigger and zero TDC, for VDC 6: 0

All events used for creating histogram for VDC 1: 0
All events used for creating histogram for VDC 2: 1063
All events used for creating histogram for VDC 3: 610
All events used for creating histogram for VDC 4: 127
All events used for creating histogram for VDC 5: 0
All events used for creating histogram for VDC 6: 1376

All events used for gauss fit (red) for VDC 1: 0
All events used for gauss fit (red) for VDC 2: 326
All events used for gauss fit (red) for VDC 3: 323
All events used for gauss fit (red) for VDC 4: 69
All events used for gauss fit (red) for VDC 5: 0
All events used for gauss fit (red) for VDC 6: 532

All events used for gauss fit (green) for VDC 1: 0
All events used for gauss fit (green) for VDC 2: 736
All events used for gauss fit (green) for VDC 3: 284
All events used for gauss fit (green) for VDC 4: 56
All events used for gauss fit (green) for VDC 5: 0
All events used for gauss fit (green) for VDC 6: 843

Ratio used for histogram / found for chamber : --- for VDC1
Ratio used for histogram / found for chamber : 0.362181 for VDC2
Ratio used for histogram / found for chamber : 0.486443 for VDC3
Ratio used for histogram / found for chamber : 0.024971 for VDC4
Ratio used for histogram / found for chamber : --- for VDC5
Ratio used for histogram / found for chamber : 0.853069 for VDC6

Ratio used for v_d calculation / found for chamber : --- for VDC1
Ratio used for v_d calculation / found for chamber : 0.361840 for VDC2
Ratio used for v_d calculation / found for chamber : 0.484051 for VDC3
Ratio used for v_d calculation / found for chamber : 0.024577 for VDC4
Ratio used for v_d calculation / found for chamber : --- for VDC5
Ratio used for v_d calculation / found for chamber : 0.852449 for VDC6

Ratio red to green peak: --- for VDC1
Ratio red to green peak: 326 : 736 = 0.442935 for VDC2
Ratio red to green peak: 323 : 284 = 1.137324 for VDC3
Ratio red to green peak: 69 : 56 = 1.232143 for VDC4
Ratio red to green peak: --- for VDC5
Ratio red to green peak: 532 : 843 = 0.631079 for VDC6

```